CARBON 49 (2011) 62–69

available at www.sciencedirect.com

ScienceDirect

journal homepage: www.elsevier.com/locate/carbon

Bending modes, elastic constants and mechanical stability of graphitic systems

G. Savini [a,b,*], Y.J. Dappe [c], S. Öberg [d], J.-C. Charlier [e], M.I. Katsnelson [a], A. Fasolino [a]

[a] Institute for Molecules and Materials, Radboud University Nijmegen, 6525ED Nijmegen, The Netherlands
[b] Department of Engineering, University of Cambridge, CB3 0FA Cambridge, United Kingdom
[c] Institut de Physique et Chimie des Matériaux, CNRS, F-67034 Strasbourg, France
[d] Department of Mathematics, Luleå University of Technology, S-97187 Luleå, Sweden
[e] Institute of Condensed Matter and Nanosciences (IMCN), Université Catholique de Louvain, Place Croix du Sud 1 (NAPS-Boltzmann), B-1348 Louvain-la-Neuve, Belgium

ARTICLE INFO

Article history:
Received 9 July 2010
Accepted 18 August 2010
Available online 24 August 2010

ABSTRACT

The thermodynamic and mechanical properties of graphitic systems are strongly dependent on the shear elastic constant C_{44}. Using state-of-the-art density functional calculations, we provide the first complete determination of their elastic constants and exfoliation energies. We show that stacking misorientations lead to a severe lowering of C_{44} of at least one order of magnitude. The lower exfoliation energy and the lower C_{44} (more bending modes) suggest that flakes with random stacking should be easier to exfoliate than the ones with perfect or rhombohedral stacking. We also predict ultralow friction behaviour in turbostratic graphitic systems.

1. Introduction

Graphitic systems are used for a wide variety of industrial applications, ranging from lubricant and refractory materials to neutron moderators in nuclear fission reactors [1] and plasma shields in the next generation of fusion reactors [2,3]. The recent realization of graphene [4] (single graphitic layer) and the discovery of its unusual electronic properties [5,6] have raised the interest on flake graphitic systems as a route to produce graphene samples of high quality and in large scale [7–9].

Despite the technological and scientific importance of graphitic systems, the knowledge of their elastic properties is unexpectedly poor and new insights are needed. The values of the elastic constants describe the mechanical behaviour [10] and are decisive in engineering design to avoid material failure. In layered materials, they are even more important for the thermodynamic properties due to a low-lying branch of acoustic vibrations, the bending modes, predicted by Lifshitz [11] over 50 years ago. Here we show that the shear elastic constant C_{44} affects the mechanism of exfoliation that is relevant for the production of graphene.

The most reliable experimental studies of the elastic constants have been obtained by inelastic X-ray scattering [12] and ultrasonic, sonic resonance, and static test methods [13]. The sample used in the first study [12] was single-crystalline Kish graphite, characterized by an extraordinary high degree of ordering, the closest approximation to the perfect AB stacking graphite (hex-g). The second study [13] was done using highly oriented pyrolitic graphite, the closest approximation to turbostratic graphite (turbo-g) where the graphitic layers are randomly oriented around the c-axis.

Except for C_{44} and C_{13}, both studies are in agreement within the experimental uncertainties. The C_{13} value in turbo-g was determined only by the less accurate static test method and it may be affected by errors. Conversely, C_{44} in turbo-g was determined from the sound velocity and its value ranges between 0.18 and 0.35 GPa [13], one order of magnitude lower than 5.0 ± 3 GPa found in hex-g [12].

* *Corresponding author at*: Department of Engineering, University of Cambridge, CB3 0FA Cambridge, United Kingdom. Fax: +44 1223 748348.
E-mail address: gs397@cam.ac.uk (G. Savini).
0008-6223/$ - see front matter
doi:10.1016/j.carbon.2010.08.042

The discrepancy on C_{44} is attributed to the existence of mobile basal dislocations [13,14]. After neutron irradiation, the elastic constant C_{44} increases by up to an order of magnitude [14], suggesting that interstitial defects [15] could pin the dislocation motions, whence the intrinsic value of C_{44} is measured. A principal difficulty with this explanation is that interstitial atoms inevitably increase the shear resistance between graphitic layers and therefore they may increase the C_{44} value by themselves.

The aim of this study is to investigate from first principles the elastic constants of graphitic systems with respect to the stacking misorientations between layers, and to describe the key role of the shear elastic constant C_{44} on the bending modes (thermal property) and mechanical stability. We show that stacking misorientations greatly affect C_{44} and that graphitic systems with perfect (hex-g) and random (turbo-g) stacking should be considered as two distinct materials described by their own elastic and thermodynamic properties.

This paper is structured as follow. In Section 2, we give a brief summary of the theoretical methods and a discussion of the LCAO-S^2 + vdW formalism to include the long-range van der Waals (vdW) interactions. The consequences of shear elastic constant C_{44} on the bending modes and mechanical stability are shown in Sections 3.1 and 3.2, respectively.

The elastic constants in the case of high-symmetric systems (hexagonal, orthorhombic, rhombohedral and AA hexagonal stackings) and for graphitic layers randomly oriented around the c-axis (turbostratic stacking) are presented in Sections 3.3 and 3.4, respectively.

Finally, we summarize and comment on our results (Section 4).

2. Method

All the calculations are performed using density functional theory, within the local density approximation scheme (LDA), norm-conserving pseudopotentials [16] and plane waves with cut-off energy of 150 Ry (ABINIT package [17]). The k-point mesh was chosen so that the average density corresponds approximately to a $32 \times 32 \times 16$ mesh for hex-g. Energies were converged within 0.05 meV/atom, and elastic constants within 0.5%. For large supercells (turbo-g with more than 50 atoms) we have used localized basis-set composed of Gaussian orbitals (AIMPRO code [18]). The elastic constants calculated by the two LDA codes are in agreement within 3% or better.

The choice of LDA is not fortuitous [19] and it was dictated by test calculations using the generalized-gradient approximation (GGA) within the Perdew–Burke–Ernzerhof scheme [20]. According to GGA, the distance between graphitic layers is far too large (4.2 Å), resulting in a negligible interlayer binding energy and almost vanishing out-of-plane elastic constants (C_{44}, C_{33}). For these reasons we have dismissed the use of GGA from this study [21–23].

Even though LDA yields accurate equilibrium distances, due to energetical error compensations, the long-range van der Waals (vdW) and more generally the weak contribution to the out-of-plane interactions is not well described [24,25]. In order to check the importance of these effects on C_{44} and C_{33}, we have used the LCAO-S^2 + vdW formalism to include these specific interactions within LDA [26] (using FIREBALL code [27]).

This formalism takes into account two major contributions. The first one, which we call weak chemical interaction, is a repulsive energy originating from the overlaps of electronic densities between the weakly interacting subsystems. Even though the overlaps are rather small, this energy is not negligible. This contribution is evaluated proceeding to a second order expansion of the electronic wavefunctions with respect to the overlaps.

The second contribution, which is the vdW itself, originating from charge fluctuations, can be seen as the interaction between electronic dipoles. In the frame of the dipolar approximation, we use a second order perturbation theory to describe this contribution. This method has originally been tested with success on standard graphene–graphene interaction, and more recently on a wide range of graphitic materials [28]. In its current stage, the analysis of the internal stresses is not implemented yet, thus the elastic constants that change the in-plane bond lengths (C_{11}, C_{12}, C_{13}) are overestimated by up to 15%. However, for C_{44} and C_{33} that describe the weak interaction between layers, the internal stresses are negligible, and the calculated values are expected to be very accurate.

The elastic constants are determined using two different approaches. The first one uses the response-function, implemented in the ABINIT code, to calculate the second derivative of the total energy with respect to the strains.

The second approach uses the elastic energy density [29]. For each elastic constant we have applied 21 strain components ε_{ij} to the equilibrium crystal structures (ε_{ij} were typically ranging between ±0.01 with increments 0.001). The elastic constants are found by fitting the calculated energies to a polynomial function in the strains. Both approaches yield results in agreement within 0.2%.

3. Results and discussion

3.1. Bending modes

The bending modes are atomic vibrations that can be excited even at low temperature and strongly influence the thermal properties of layered materials. In 1952, Lifshitz [11] obtained the following dispersion law for the out-of-plane acoustic mode ω:

$$\rho \times \omega^2(q) = C_{44}\left(q_x^2 + q_y^2\right) + C_{33}\left(q_z^2\right) + \kappa\left(q_x^2 + q_y^2\right)^2/c \qquad (1)$$

where ρ is the density, c is the interlayer distance, $q_{x,y,z}$ are the wave vectors and κ describes the intralayer forces characterizing the bending rigidity (1.1 eV [30]). The small value of C_{44} (characteristic of graphitic systems, see Table 1) leads to a predominant contribution of the transversal bending modes ($q_z = 0$) in the phonon dispersion curves. These modes are sinusoidal displacements that propagate along the planes and change the local stacking between layers (see Fig. 1). For nearly flat planes the shear stacking Δd is almost zero, whereas, for positive (or negative) slope Δd becomes positive (or negative). Using trigonometric considerations, it can be shown that the maximum value of Δd (see boxes in Fig. 1) is given by:

Table 1 – Elastic constants in unit of GPa for the different graphitic systems. The values between brackets are calculated using the van der Waals correction. These results show that the C_{13} values do not significantly change between turbo-g and hex-g and we propose that the same value 0 ± 3 GPa should be appropriate also for turbostratic stacking. The shear elastic constants C_{44} found in turbostratic stacking correspond to commensurate structures of area ranging between 36 and 563 Å^2.

		C_{11}	C_{12}	C_{33}	C_{13}	C_{44}
Hex-g (AB)	Exp. [12]	1109 ± 16	139 ± 36	38.7 ± 7	0 ± 3	5.0 ± 3.0
	Theory	1109	175	29 (42)	−2.5	4.5 (4.8)
Turbo-g	Exp. [13]	1060 ± 20	180 ± 20	36.5 ± 1	15 ± 5	0.18/0.35
	Theory	1080 ± 3	171 ± 4	27 ± 2 (36 ± 1)	−2.7 ± 1	0.16/0.31 (0.19/0.34)
Rhombo-g	Theory	1107	175	29 (42)	−2.5	4.4 (4.8)
Ortho-g	Theory	1095	173	26 (38)	−2.6	−2.7/7.7 (−2.9/7.3)
Hex-g (AA)	Theory	1028	162	21 (30)	−3.0	−3.8 (−3.8)

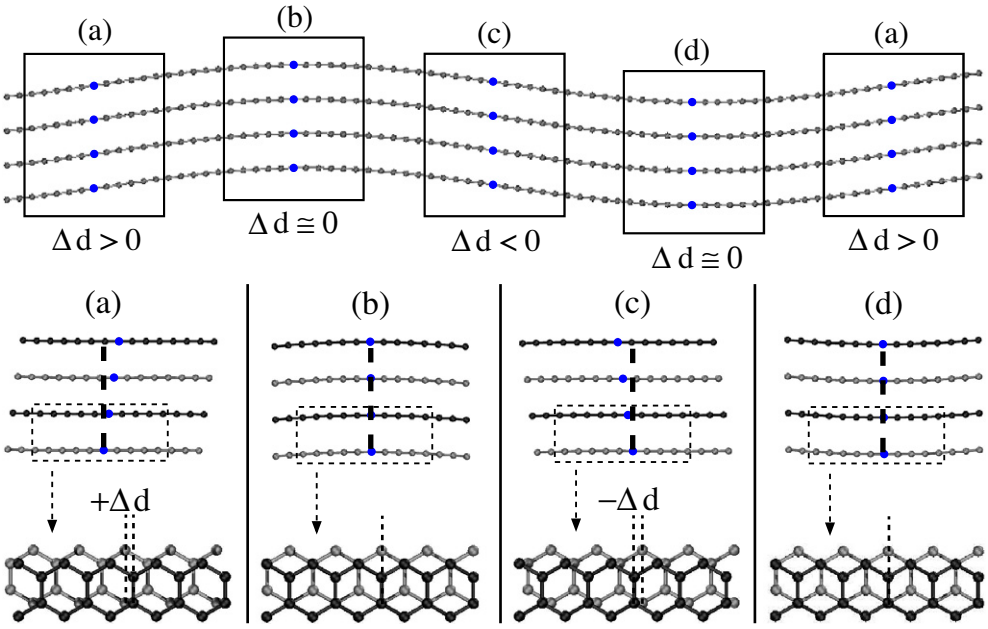

Fig. 1 – Transversal acoustic (bending) mode. The bending changes the local stacking between graphitic layers. The boxes (a–d) show regions with different slopes and stackings. The shear Δd gives the deviations from AB phase (perfect stacking).

$$\Delta d = \frac{\pi \hat{a} c}{\lambda} \times \frac{1}{\sqrt{1 + \left(\frac{2\pi\hat{a}}{\lambda}\right)^2}} \quad (2)$$

where $\hat{a}$ is the amplitude, λ is the wavelength and c is the interlayer distance. The crystal resistance to the stacking shear [29] is proportional to $E \propto C_{44} \times \Delta d^2$, and by lowering C_{44} more bending modes can be excited at lower temperature. In the limit of $C_{44} = 0$, graphitic systems approach the graphene behaviour, where indeed bending modes (or ripples) are always present [30].

3.2. *Mechanical stability*

By imposing the elastic strain energy as positively definite [29], the stability conditions are given by:

$$2C_{13}^2 < C_{33}(C_{11} + C_{12}) \text{ and } C_{11}, C_{12}, C_{33}, C_{44} > 0 \quad (3)$$

Note that C_{13} does not affect the stability: a positive (or negative) value means that under in-plane compression the out-of-plane distance tends to expand (or contract).

The elastic constants C_{11}, C_{12} describe in-plane deformations and they possess the highest values due to the strong sp^2 bonding interactions within the graphene planes. The elastic constant C_{33} describes out-of-plane compression or expansion and it has always a positive value for perfect and stacking misorientations (see Table 1).

The elastic constant C_{44} corresponds to a shear between graphene layers. Due to the weak interaction between planes, the C_{44} value is the lowest and can be positive or negative depending on the stacking misorientations (see Table 1). The latter elastic constant is the only one that can break the mechanical stability condition (*i.e.* $C_{44} < 0$).

3.3. *Elastic constants in high-symmetric graphitic systems*

By imposing a translation vector between graphitic layers we found four high-symmetric stackings that correspond to stationary points on the stacking-fault energy surface [31]. To calculate the stacking-fault energy surface (for graphitic

system is often called corrugation energy surface [32–34]), we have used 16-atoms unit cell model of eight layers in AB sequence in which the stacking at the unit cell boundary is changed by imposing a shear displacement. This represents an intrinsic stacking fault between layers at the unit cell boundaries whereas the others remains stacked in the AB sequence. The multiple layers repeat along the c-axis (eight layers) makes negligible self-interaction of the intrinsic fault [31]. The stationary points, indicated with square and circle symbols in Fig. 2a, correspond to the four high-symmetric structures (hexagonal, rhombohedral, orthorhombic and AA hexagonal graphite, see Fig. 2b). The in-plane lattice parameter was 2.45 Å very close to the experimental value 2.463 Å [12], with no significant changes among all the graphitic structures.

The origin in Fig. 2a corresponds to hex-g (black square symbol), the global minimum of the energy surface with an interlayer separation of 3.34 Å (experimental value 3.356 Å [12]). With the exception of the C_{33} value (29 GPa), the calculated elastic constants (given in Table 1) are in agreement within the experimental uncertainties found in hex-g [12]. Using the LCAO-S^2 + vdW formalism, the out-of-plane elastic constant C_{33} becomes 42 GPa, very close to the experimental value 38.7 ± 7 GPa [12].

The local minimum at $1/3\langle 1\bar{1}00\rangle$ (black circle symbol) represents the rhombohedral stacking (rhombo-g). This structure possesses the same interlayer separation and elastic constants of hex-g (the differences are beyond the accuracy of the calculations) with formation energy of 0.10 meV/atom. This very small energy explains why the rhombohedral phase is usually 5–15% intermixed with the perfect hexagonal one in natural graphitic flakes.

The saddle point at $1/6\langle 1\bar{1}00\rangle$ (grey square symbol) represents the orthorhombic stacking (ortho-g). The interlayer separation of the primitive unit cell is 3.37 Å with formation energy of 1.66 meV/atom. The latter energy represents the lowest barrier that has to be overcome during the shearing process from an ideal configuration to another equivalent one. The C_{44} values are found to range between −2.7 GPa, for shearing along $\langle 1\bar{1}00\rangle$ and 7.7 GPa, for shearing along

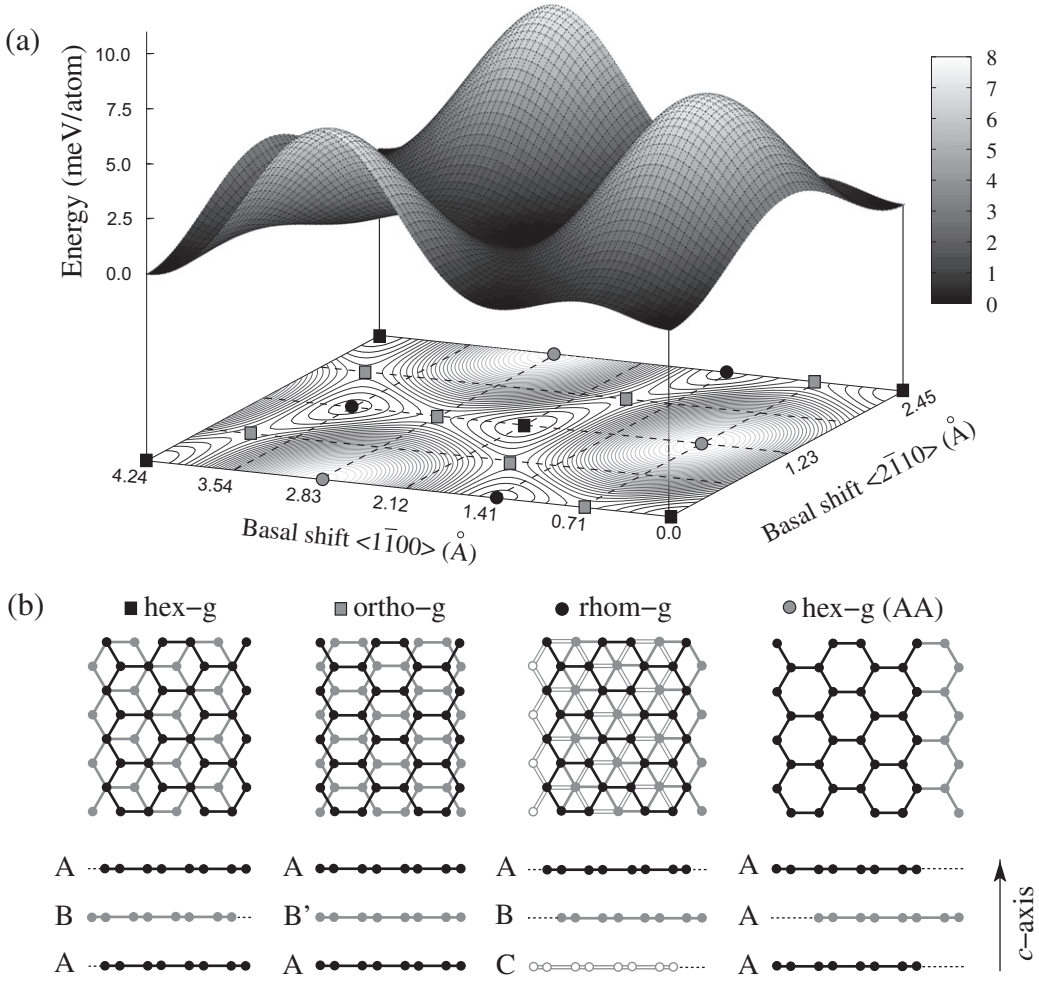

Fig. 2 – (a) Stacking-fault energy surface (also called corrugation energy surface). The square and circle symbols indicate the stationary points corresponding to the following high-symmetric structures; (b) The hexagonal, orthorhombic, rhombohedral and AA hexagonal stackings viewed perpendicular (above), parallel (below) to the c-axis. The energies of these structures with respect to hex-g are 1.66 meV/atom for ortho-g, 0.10 meV/atom for the rhom-g and 9.29 meV/atom for AA hex-g (see text).

the $\langle 2\bar{1}10\rangle$ axis. No significant changes are found for the other elastic constants (see Table 1). Although unstable (due to the negative C_{44}), this structure acts as an intermediate phase during the transformation from graphite to diamond [35].

The global maximum at $2/3\langle 1\bar{1}00\rangle$ (grey circle symbol) corresponds to AA hexagonal stacking (AA hex-g). This phase has the largest interlayer separation (3.60 Å) and the highest formation energy (9.29 meV/atom). Its elastic constants are smaller than in hex-g, and C_{44} in particular, becomes negative (−3.8 GPa) breaking the stability conditions. Even though this structure is highly unstable, a recent study has suggested that screw dislocations locally encourage this stacking [36].

In the following section we describe the elastic constants for graphitic layers randomly oriented around the *c*-axis.

3.4. *Elastic constants in turbostratic stacking*

The modelling of turbostratic staking is challenging since the incommensurate nature of these stackings must combine with the finite-size constraint required by calculations. To overcome this difficulty we used the method proposed by Kolmogorov and Crespi [32] in which a layer with supercell basis vector (n, m) becomes commensurate with a second layer for a specific rotation angle of:

$$\vartheta = \cos^{-1}\left[\frac{2n^2 + 2nm - m^2}{2(n^2 + nm + m^2)}\right] \quad \text{with } n > m \tag{4}$$

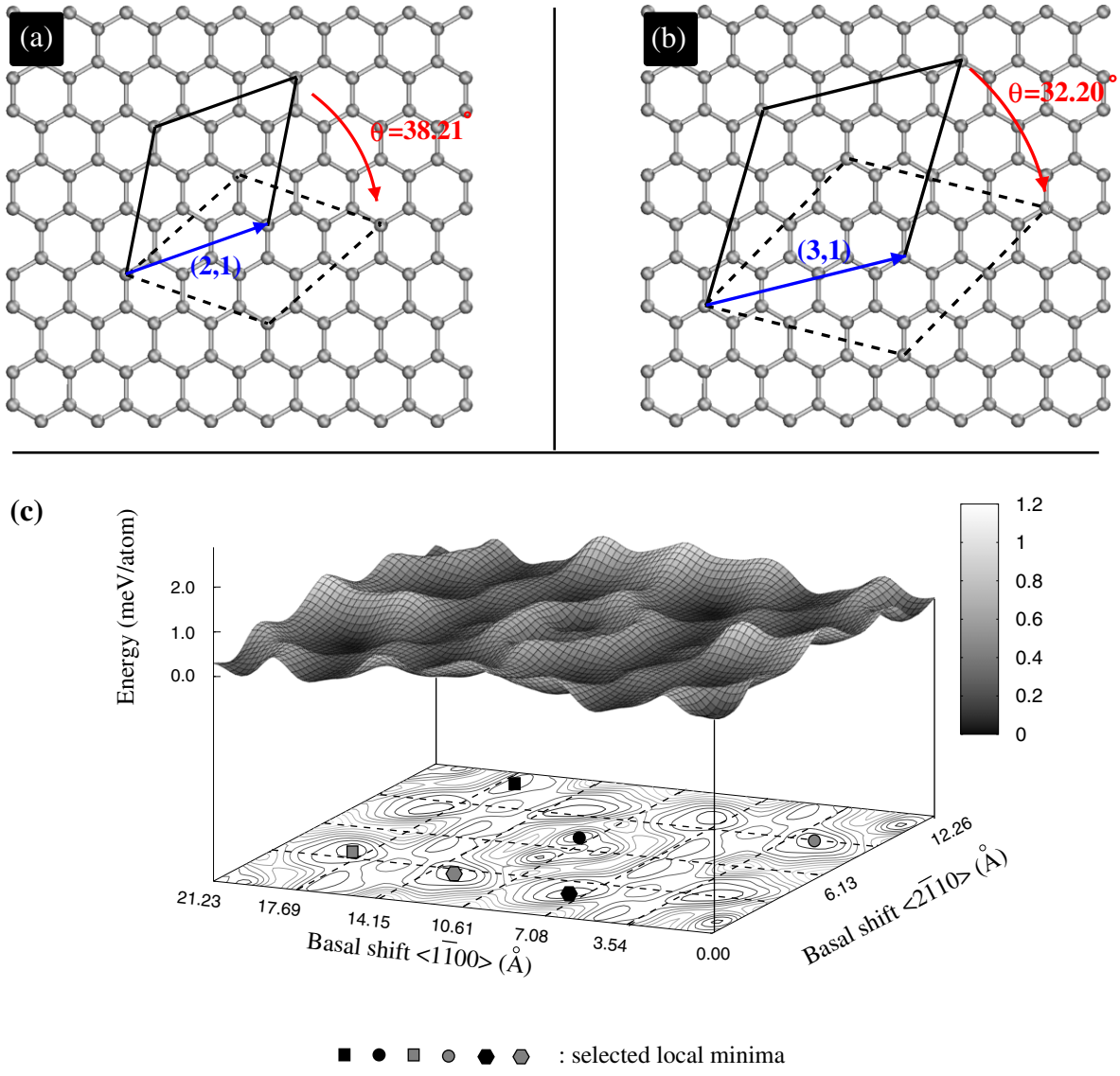

Fig. 3 – (a and b) Representation of accidental commensuration. A supercell of vector *n*, *m* (blue colour) becomes commensurate when rotated by an angle ϑ with respect to the starting supercell (as we increase *n*, *m* the supercell surface and number of atoms rapidly increase). (c) Stacking-fault energy surface (or corrugation energy surface) of a graphene bilayer with supercell vector 2, 1. The respective elastic constants are calculated on the local minima of the energy surface. Notice that the energy surface becomes much flatter leading to a reduction of C_{44}. (For interpretation of the references to colour in this figure legend, the reader is referred to the web version of this article.)

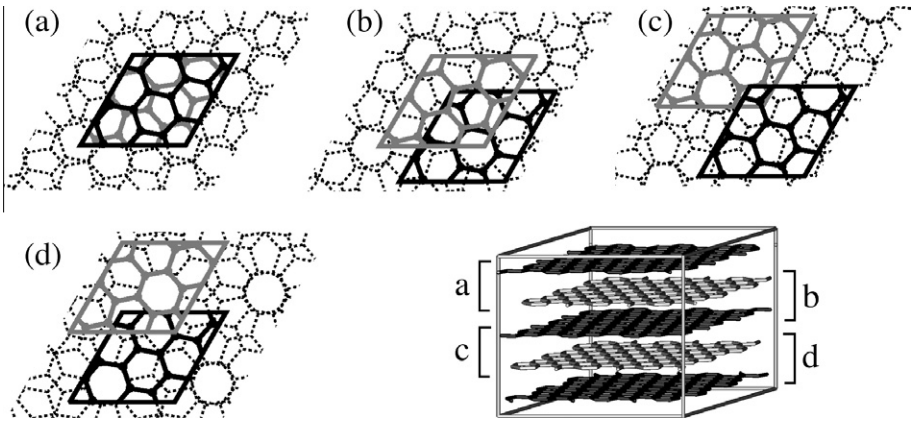

Fig. 4 – An example of five layers turbostratic stacking (supercell basis vector 2,1). Each layer is stacked along the c-axis, rotated with respect to each other with an angle of 38.21° and randomly translated along the basal plane.

Fig. 3a and b shows the case of the two smaller supercell with basis vector $2,1$ and $3,1$ (corresponding to 14, 26 atoms/layer and rotation angles of 38.21°, 32.20°, respectively). Fig. 3c shows the stacking energy surface for a bilayer supercell of basis vector $2,1$. To better describe the complete misorientation of turbostratic stacking we have increased the number of layers along the *c*-axis. Each layer was rotated with respect to each other and randomly translated along the basal plane (see Fig. 4). The rotation angles used are 15 values ranging from 6.01° to 53.99°. The smallest supercell contains 28 atoms with two layers rotated with respect to each other by 38.21°, whereas the largest one contains 456 atoms with 12 layers and rotation angle of 46.83°.

For each model we carried out extensive structural optimizations starting from different translation vectors along the basal plane. The corrugation energy is about one order of magnitude lower than commensurate structure (see Fig. 2a) with a maximum value of 0.9 meV/atom (see Fig. 3c). As we increased the size of the supercell over the basal plane we found that the average corrugation energy tends to decrease up to 20% for the largest size (basis vector 8,3 with 194 atoms/layer). Extrapolating these results in the ideal case of infinite layers, we suggest corrugation energy virtually flat with layers mutual independent.

For all the supercell studied the in-plane lattice parameters remain almost equal to the value found in hex-g, whereas the interlayer distances were on average slightly larger, 3.42 ± 0.01 Å, with formations energies of 3.03 ± 0.6 meV/atom.

The interlayer binding energy between graphitic layers (*i.e.* exfoliation energy) was 21 ± 1 meV/atom (70 ± 4 meV/atom with vdW), a value slightly lower than the 24 meV/atom found in hex-g (80 meV/atom with vdW). Note that LDA values yield to a binding energy within a factor of 2–3 with respect to LCAO-S^2 + vdW formalism and experiment values (43 meV/atom found in heat-of-wetting experiment [37], 35 ± 10 meV/atom found by analyzing TEM images of twisted collapsed nanotubes [38], and 52 ± 5 meV/atom by studying thermal desorption of polyaromatic hydrocarbons [39]). In Table 1 we report the calculated values of the elastic constants. With the exception of C_{44}, these values hardly change among all the studied turbostratic stackings with no clear dependence on the rotation angles and number of layers. The elastic constants C_{11}, C_{12} slightly decrease by about 3% with respect to hex-g, remaining within the experimental uncertainties found in turbostratic samples [13]. As previously found in hex-g, LDA calculations underestimate the C_{33} value (27 ± 2 GPa) with respect to the vdW correction (36 ± 1 GPa) and the experimental value of 36.5 ± 1 GPa [13].

Conversely, we found $C_{13} = -2.7 \pm 0.5$ GPa in disagreement with the experimental value 15 ± 5 GPa [13]. The latter value was only indirectly obtained as a function of the other elastic constants by the less accurate static test method. This method requires larger strains than ultrasonic experiments and non-linear behaviour of stress–strain curve may affect the measured value. Furthermore, the linear bulk modulus B_a calculated from these elastic constants is far too large (2080 GPa), almost double than the one found in diamond (1326 GPa [40]).

The linear bulk modulus B_a describes the variation of the lattice parameter *a* as a function of the hydrostatic pressure [41] and it is given by:

$$B_a = \frac{C_{33}(C_{11} + C_{12}) - 2C_{13}}{C_{33} - C_{13}} \tag{5}$$

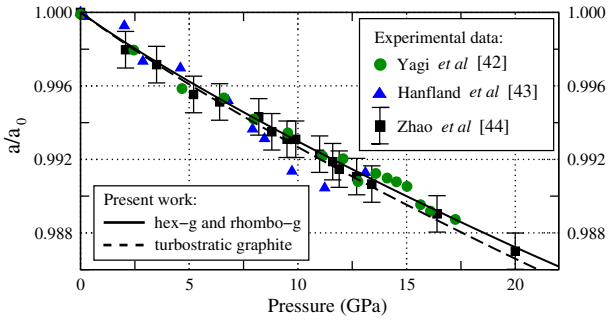

Fig. 5 – In-plane lattice parameters vs. pressure. The solid line represents the results found for hex-g and rhombo-g (perfect and rhombohedral stackings). The dashed line shows the results found here for turbostratic graphite. For comparison, the experimental results are also plotted.

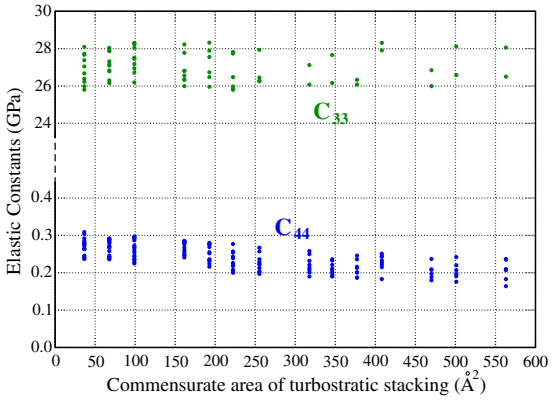

Fig. 6 – The elastic constants C_{44} and C_{33} as a function of the commensurate area over the basal plane in turbostratic stacking. The C_{44} value tends to decrease with respect to the supercell size, whereas C_{33} is not quantitatively affected.

This modulus is strongly weighted by C_{13}. For example, if we use the measured value found in hex-g 0 ± 3 GPa (instead of 15 ± 5 GPa), B_a becomes 1240 GPa (instead of 2080 GPa).

Several X-ray studies have measured the linear bulk modulus B_a. In these experiments powder samples were prepared by grinding different types of graphitic materials, ranging from well crystallized to poorly crystallized grains [42–44]. The good agreement between the experiments (see Fig. 5) indicates that the linear bulk modulus B_a does not strongly depend on the stacking order with a measured value of 1250 ± 70 GPa [43]. By including the latter modulus in the Eq. (5), the elastic constant C_{13} becomes 0.3 GPa. Therefore, we conclude that the C_{13} value does not significantly change between turbo-g and hex-g and we propose that the same value 0 ± 3 GPa should be appropriate also for turbostratic stacking.

The C_{44} represents the second derivative of the total energy as a function of shear displacement over the basal plane. As the corrugation energy of perfect AB stacking is much higher than turbostratic we are expecting a corresponding lower value of the shear elastic constant. We have found that C_{44} tends to decrease as a function of the supercell area over the basal plane (see Fig. 6) and is independent on the relative rotation angles and number of layers along the c-axis (the respective average corrugation energies and therefore the C_{44} values are also independent on the relative rotation angles and number of layers).

For commensurate structures of finite area ranging between 36–563 Å^2 the respective C_{44} values are within 0.16–0.31 GPa, one order of magnitude lower than hex-g (4.5 GPa) and close to the experimental measures ranging from 0.18 to 0.35 GPa [13]. The vdW correction does not significantly affect the C_{44} values with respect to LDA (see Table 1), suggesting that the variations in energy under interlayer shears are nearly identical between these two approximations. As we increase the sizes of the commensurate structures towards the ideal case of infinite layers (incommensurate) the C_{44} values tend to zero with corrugation energy virtually flat. These results indicate that turbostratic stacking possesses the lowest friction among all the graphitic materials bearing great potential applications in nano-mechanical systems [45,46].

4. Conclusions

To summarize, we have discussed the importance of C_{44} as the main parameter that restrains the bending modes and controls the mechanical stability of layered materials. Using advanced *ab initio* method, which includes vdW interactions, we have provided the first complete description of the elastic constants in graphitic systems. The lower exfoliation energy (~10 meV/atom) and the lower C_{44} (at least one order of magnitude) found in turbostratic stacking suggest that the exfoliation mechanism, relevant for the production of graphene, should be easier for graphite flakes with random stacking.

Our results indicate that turbostratic graphitic systems possess the lowest friction among all the graphitic stackings. It would be interesting to check these predictions experimentally.

Acknowledgements

The authors thank the HPC-EUROPA project for financial and computer supports. Computational resources have also been provided by the Université Catholique de Louvain on the LEMAITRE and GREEN computers of the CISM. JCC acknowledges financial support from the FRS-FNRS of Belgium; GS from JSPS and Grant-in-Aid for Scientific Research.

REFERENCES

[1] Klimenkov VI. Behavior of graphite in nuclear reactor stacks. Atom Energy 1962;10(5):439–50.
[2] Evans TE, Moyer RA, Burrell KH, Fenstermacher ME, Joseph I, Leonard AW, et al. Edge stability and transport control with resonant magnetic perturbations in collisionless tokamak plasmas. Nature Phys 2006;2:419–23.
[3] Scaffidi-Argentina F, Safronov V, Arkhipov I, Arkhipov N, Bakhtin V, Barsuk V, et al. Erosion mechanisms and products in graphite targets under simulated disruption conditions. J Nucl Mater 2000;283–287(2):1111–5.
[4] Novoselov KS, Geim AK, Morozov SV, Jiang D, Zhang Y, Dubonos SV, et al. Electric field effect in atomically thin carbon films. Science 2004;306(5696):666–9.
[5] Novoselov KS, Geim AK, Morozov SV, Jiang D, Katsnelson MI, Grigorieva IV, et al. Two-dimensional gas of massless Dirac fermions in graphene. Nature 2005;438:197–200.
[6] Zhang Y, Tan Y, Stormer HL, Kim P. Experimental observation of the quantum Hall effect and Berry's phase in graphene. Nature 2005;438:201–4.
[7] Li X, Wang X, Zhang L, Lee S, Dai H. Chemically derived, ultrasmooth graphene nanoribbon semiconductors. Science 2008;319:1229–32.
[8] Hernandez Y, Nicolosi V, Lotya M, Blighe FM, Sun Z, De S, et al. High-yield production of graphene by liquid-phase exfoliation of graphite. Nature Nanotechnol 2008;3:563–8.
[9] Siegel DA, Hwang CG, Fedorov AV, Lanzara A. Quasifreestanding multilayer graphene films on the carbon face of SiC. Phys Rev B 2010;81. 241417–4.
[10] Mohiuddin TMG, Lombardo A, Nair RR, Bonetti A, Savini G, Jalil R, et al. Uniaxial strain in graphene by Raman spectroscopy: G peak splitting, Grüneisen parameters, and sample orientation. Phys Rev B 2009;79(20):205433–8.

[11] Lifshitz IM. On the thermal properties of chain and layered structures at low temperatures. Zh Eks Teor Fiz 1952;22(4):475–86.
[12] Bosak A, Krisch M, Mohr M, Maultzsch J, Thomsen C. Elasticity of single-crystalline graphite: inelastic X-ray scattering study. Phys Rev B 2007;75(15). 153408–4.
[13] Blakslee OL, Proctor DG, Seldin EJ, Spence GB, Weng T. Elastic constants of compression-annealed pyrolytic graphite. J Appl Phys 1979;41(8):3373–82.
[14] Seldin EJ, Nezbeda CW. Elastic constants and electron-microscope observations of neutron-irradiated compression-annealed pyrolytic and single-crystal graphite. J Appl Phys 1970;41(8):3389–400.
[15] Suarez-Martinez I, El-Barbary AA, Savini G, Heggie MI. First-principles simulations of boron diffusion in graphite. Phys Rev Lett 2007;98(1):015501–4.
[16] Troullier N, Martins JL. Efficient pseudopotentials for plane-wave calculations. II. Operators for fast iterative diagonalization. Phys Rev B 1991;43(11):8861–9.
[17] Gonze X, Beuken J-M, Caracas R, Detraux F, Fuchs M, Rignanese G-M, et al. First-principles computation of material properties: the ABINIT software project. Comput Mater Sci 2002;25(3):478–92.
[18] Briddon PR, Jones R. LDA calculations using a basis of gaussian orbital. Phys Stat Sol (b) 2000;217(1):131–71.
[19] Perdew JP, Zunger A. Self-interaction correction to density-functional approximations for many-electron systems. Phys Rev B 1981;23(10):5048–79.
[20] Perdew JP, Burke K, Ernzerhof M. Generalized gradient approximation made simple. Phys Rev Lett 1996;77(18):3865–8.
[21] Tournus F, Charlier J-C, Melinon P. Mutual orientation of two C60 molecules: an *ab initio* study. J Chem Phys 2005;122(9):094315–9.
[22] Charlier J-C, Gonze X, Michenaud J-P. First-principles study of the stacking effect on the electronic properties of graphite(s). Carbon 1994;32(2):289–99.
[23] It is clear that GGA (leading to a distance of 4.2 Å and energy of 2–3 meV/atom) seriously underestimates the interlayer binding energy and is in strong disagreement for the geometry. Thus, even if LDA is unable to describe the dispersion interactions, it is a better choice than the GGA as far as the geometry and energy differences are concerned.,
[24] Mounet N, Marzari N. First-principles determination of the structural, vibrational and thermodynamic properties of diamond, graphite, and derivatives. Phys Rev B 2005;71(20). 205214–14.
[25] Charlier J-C, Gonze X, Michenaud J-P. Graphite interplanar bonding: electronic delocalization and van der Waals interaction. Europhys Lett 1994;28(6):403–8.
[26] Dappe YJ, Basanta MA, Flores F, Ortega J. Weak chemical interaction and van der Waals forces between graphene layers: a combined density functional and intermolecular perturbation theory approach. Phys Rev B 2006;74(20):205434–9.
[27] Lewis JP, Glaesemann KR, Voth GA, Fritsch J, Demkov AA, Ortega J, et al. Further developments in the local-orbital density-functional-theory tight-binding method. Phys Rev B 2001;64(19):195103–10.
[28] Dappe YJ, Ortega J, Flores F. Intermolecular interaction in density functional theory: application to carbon nanotubes and fullerènes. Phys Rev B 2009;79(16): 165409–10.
[29] Born M, Huang K. Dynamical Theory of Crystal Lattices. New York: Oxford University Press; 1954.
[30] Fasolino A, Los JH, Katsnelson MI. Intrinsic ripples in graphene. Nature Mater 2007;6:858–61.
[31] Kaxiras E, Duesbery MS. Free energies of generalized stacking faults in Si and implications for the brittle-ductile transition. Phys Rev Lett 1993;70(24):3752–5.
[32] Kolmogorov AN, Crespi VH. Registry-dependent interlayer potential for graphitic system. Phys Rev B 2005;71(23):235415–6.
[33] Kolmogorov AN, Crespi VH. Smoothest bearings: interlayer sliding in multiwalled carbon nanotubes. Phys Rev Lett 2000;85(22):4727–30.
[34] Kolmogorov AN, Crespi VH, Schleier-Smith MH, Ellenbogen JC. Nanotube-substrate interactions: distinguishing carbon nanotubes by the helical angle. Phys Rev Lett 2004;92(8):085503–4.
[35] Scandolo S, Bernasconi M, Chiarotti GL, Focher P, Tosatti E. Pressure-induced transformation path of graphite to diamond. Phys Rev Lett 1995;74(20):4015–8.
[36] Suarez-Martinez I, Savini G, Haffenden G, Campanera J-M, Heggie MI. Dislocations of burgers vector c/2 in graphite. Phys Stat Sol (c) 2007;4(8):2958–62.
[37] Girifalco LA, Ladd RA. Energy of cohesion, compressibility, and the potential energy functions of the graphite system. J Chem Phys 1956;25:693–7.
[38] Benedict LX, Chopra NG, Cohen ML, Zettl A, Louie SG, Crespi VH. Microscopic determination of the interlayer binding energy in graphite. Chem Phys Lett 1998;286(5–6): 490–6.
[39] Zacharia R, Ulbricht H, Hertel T. Interlayer cohesive energy of graphite from thermal desorption of polyaromatic hydrocarbons. Phys Rev B 2004;69(15):155406–7.
[40] Grimsditch MH, Ramdas AK. Brillouin scattering in diamond. Phys Rev B 1975;11(8):3139–48.
[41] Schreiber E, Anderson OL, Soga N. Elastic Constants and Their Measurement. New York: McGraw-Hill; 1973.
[42] Yagi T, Utsumi W, Yamakata M, Kikegawa T, Shimomura O. High-pressure *in situ* X-ray-diffraction study of the phase transformation from graphite to hexagonal diamond at room temperature. Phys Rev B 1992;46(10):6031–9.
[43] Hanfland M, Beister H, Syassen K. Graphite under pressure: equation of state and first-order Raman modes. Phys Rev B 1989;39(17):12598–603.
[44] Zhao YX, Spain IL. X-ray diffraction data for graphite to 20 GPa. Phys Rev B 1989;40(2):993–7. to estimate *Ba* they inadvertently used the planar bulk modulus instead of using the linear one (see Schreiber et al. [41]).
[45] Dienwiebel M, Verhoeven GS, Pradeep N, Frenken JWM, Heimberg JA, Zandbergen HW. Superlubricity of graphite. Phys Rev Lett 2004;92(12):126101–4.
[46] Cumings J, Zettl A. Low-friction nanoscale linear bearing realized from multiwall carbon nanotubes. Science 2000;289(5479):602–4.